BIOCHEMISTRY
including biophysical chemistry & molecular biology

Article

pubs.acs.org/biochemistry

Kinetic Mechanism of Active Site Assembly and Chemical Catalysis of DNA Polymerase β

Paul B. Balbo,[†] Eric Chun-Wei Wang,[†,‡] and Ming-Daw Tsai*[,†,‡]

[†]Institute of Biological Chemistry, Academia Sinica, Nangang, Taipei 115, Taiwan

[‡]Institute of Biochemical Sciences, National Taiwan University, Taipei 106, Taiwan

Supporting Information

ABSTRACT: It has been inferred from structural and computational studies that the mechanism of DNA polymerases involves subtle but important discrete steps that occur between binding and recognition of the correct dNTP and chemical catalysis. These steps potentially include local conformational changes involving active site residues, reorganization of Mg^{2+}-coordinating ligands, and proton transfer. Here we address this broad issue by conducting extensive transient state kinetic analyses of DNA polymerase β (Pol β). We also performed kinetic simulations to evaluate alternative kinetic models. These studies provide some support for two-step subdomain closing and define constraints under which a kinetically significant prechemistry step can occur. To experimentally identify additional microscopic steps, we developed a stopped flow absorbance assay to measure proton formation that occurs during catalysis. These studies provide direct evidence that formation of the enzyme-bound 3′-O^- nucleophile is rate determining for chemistry. We additionally show that at low pH the chemical step is rate limiting for catalysis, but at high pH, a postchemistry conformational step is rate limiting due to a pH-dependent increase in the rate of nucleotidyl transfer. Finally, we performed exhaustive analyses of $[Mg^{2+}]$ and pH effects. In contrast to published studies, the results suggest an irregular pH dependence of k_{pol}, which is consistent with general base catalysis involving cooperativity between two or more protonic residues. Overall, the results represent significant advancement in the kinetic mechanism of Pol β and also reconcile some computational and experimental findings.

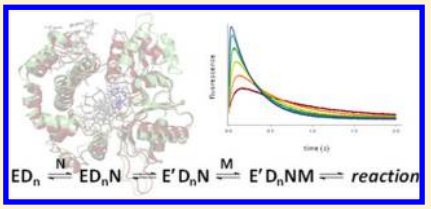

DNA polymerase β (Pol β), a moderate-to-high fidelity polymerase, exhibiting error frequencies of 10^{-4}–10^{-5},[1,2] is responsible for DNA synthesis in the DNA base excision repair pathway in eukaryotes.[3,4] Specific DNA Pol β mutants with decreased fidelity have been identified in tumor cells.[5] Moreover, Pol β is the archetypal member of the DNA Pol X family that includes DNA polymerases involved in non-homologous end joining (Pol λ, Pol σ, Pol μ), viral repair polymerases (e.g., ASFV Pol X), template-independent polymerases such as terminal deoxynucleotidyl transferase (TdT), CCA-adding enzyme, and poly(A) and poly(U) polymerases.[6] Pol β utilizes a "two metal ion" mechanism for catalysis of nucleotidyl transfer chemistry which is conserved for all DNA and RNA polymerases.[7,8]

On the basis of kinetic[9−13] and structural studies[14,15] from several laboratories, a common mechanism for DNA polymerases has been proposed (Scheme 1). This involves [1] binding of Mg·dNTP^{2-} to the enzyme−DNA binary complex to form an open ternary complex, [2] the global conformational rearrangement of subdomains to form a closed ternary complex, [3] subsequent binding of the catalytic Mg^{2+} ion, [4] the chemistry step (i.e., nucleotidyl transfer), [5] Mg^{2+} dissociation from the enzyme−product ternary complex, [6] subdomain reopening, and [7] pyrophosphate (Mg·PP$_i^{2-}$) dissociation. [In Scheme 1, E, N, P, and M refer to Pol β (enzyme), Mg·dNTP^{2-}, Mg·PP$_i^{2-}$, and Mg^{2+}, respectively, and E′ designates the enzyme in the closed subdomain conformation.] Several studies demonstrate that, for Pol β, the open-to-closed subdomain motion [step 2] is rapid relative to the overall rate of single turnover,[11,13,16−18] and additional kinetic studies[19−22] support that chemistry [step 4] is rate determining.

Despite the abundance of structural and kinetic information, the chemical and biophysical basis for polymerase activity and fidelity—and of different fidelities exhibited by different polymerases—is not well understood. Several mechanistic proposals have recently been advanced based primarily on computational[23−27] and structural[15,28] studies. The common thread in these proposals is the purported existence of additional reaction steps, particularly conformational steps involved in organization of the active site prior to chemistry. There is strong consensus that active site assembly entails Mg^{2+} binding and consequent structural reorganization such as Mg^{2+} coordination by the 3′-OH of DNA and possibly subtle adjustment of protein side chains.[28] The implication is that these conformational steps may be rate determining in enzyme catalysis and that incorrect nucleotide incorporation may be characterized by altered kinetics of these steps or, alternatively, by the formation of a suboptimal active site structure.[26,27,29] Furthermore, nucleotidyl transfer is believed to involve general

Received: June 22, 2011
Revised: September 19, 2011
Published: October 19, 2011

Scheme 1. Kinetic Mechanism of Pol β

$$ED_n \overset{N}{\rightleftharpoons} ED_nN \rightleftharpoons E'D_nN \overset{M}{\rightleftharpoons} E'D_nNM \rightleftharpoons E'D_{n+1}PM \underset{M}{\rightleftharpoons} E'D_{n+1}P \rightleftharpoons ED_{n+1}P \underset{P}{\rightleftharpoons} ED_{n+1}$$

step: [1] [2] [3] [4] [5] [6] [7]

base catalysis, and a likely candidate for this base is the carboxylate of a conserved acid residue (D256 in Pol β), based on its proximity to the 3′-OH group, or possibly an active site bound water[25,30,31] (Figure 1). Quantum mechanical (QM)-based

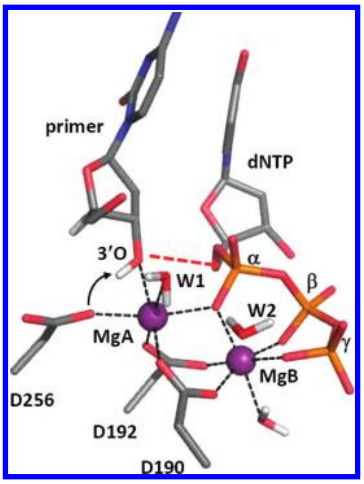

Figure 1. Active site of Pol β. The geometry of the ligands around both metals, MgA (catalytic) and MgB (dNTP-bound), is shown, including the three conserved acidic residues (D190, D192, and D256). Indicated are the hypothetical proton abstraction by D256, (black arrow), the trajectory of the 3′-O for nucleophilic attack (red dashed arrow), and metal-coordination bonds (black dashed lines). Phosphorus positions (α, β, γ) of the dNTP are labeled. Two waters are indicated: W1 is coordinated to MgA, and W2 is proximal to the triphosphate moiety of dNTP; both have been implicated in proton shuttling networks (e.g., refs 33 and 56). The model is derived from the determined structure, ref 28, of the Pol β ternary complex (pdb: 2FMS).

modeling studies[23,24,32,33] of the Pol β active site have considered various mechanisms of proton transfer and the extent to which discrete steps—including proton abstraction from the DNA 3′-OH, nucleophilic attack by the 3′-O^- on the P_α, and pyrophosphate elimination—are rate determining. It has also been proposed that correctly paired dNTPs are bound in a series of conformational steps which, together with active site assembly, constitute "kinetic checkpoints".[25] To date, many of these issues have not been experimentally verified.

The purpose of this study is to evaluate alternative kinetic mechanisms of Pol β with a particular focus on possible additional kinetic steps involved in dNTP binding, correct base-pair recognition, and assembly of the active site prior to chemical catalysis. We have employed a combination of transient state kinetic analyses and kinetic simulation studies. Our kinetic results are consistent with—but do not demand—a mechanism having a rate-determining prechemistry step. However, because various models involving prechemistry pathways having alleged importance in polymerase activity and fidelity have been strongly advocated in the literature,[24,25,28,33] we performed kinetic simulations to evaluate these hypotheses. These simulations define a range of rate constants for a putative prechemistry step that are consistent with the data, thus providing insight into possible mechanisms. In addition, the rate of enzyme-catalyzed proton formation was directly measured using a newly developed stopped flow absorbance assay and compared with the rate of nucleotidyl transfer as measured by both stopped flow fluorescence and rapid quench. These studies provide direct evidence that formation of the nucleophile (3′-O^-) is a rate-determining step in single nucleotide incorporation and further suggest a sequential mechanism whereby proton transfer precedes nucleotidyl transfer. Finally, our exhaustive pH- and [Mg]-dependence studies have led to new insight into the mechanism of nucleotidyl transfer.

MATERIALS AND METHODS

Materials. All chemicals were of analytical quality. Recombinant wild-type rat Pol β was expressed and purified as described.[34] HPLC-purified DNAs were from IDT (Coralville, IA). Stopped flow kinetic and other experiments monitoring 2AP fluorescence utilized either a 28-mer: 5′-(p)-GTGGCGAAGC-CACXTGCTGCGAAGCAGC-3′, or 29-mer DNA: 5′-(p)-GTGGCGAAGCCACXTGCTGCGAAGCAGCA-3′, where (p) is a 5′-phosphoryl group, **T** is the template deoxythymidine, and X is deoxy-2-aminopurine, designated in the text as substrate (D_n) or product (D_{n+1}) DNA, respectively. Stopped flow absorbance, related stopped flow kinetic (monitoring intrinsic Trp fluorescence emission), and rapid quench experiments utilized a 29-mer, 1-nucleotide gapped DNA: 5′-(p)-GGTGGCGAAGCCACC**T**GCTGCGAAGCAGC-3′. Some experiments, as indicated in the text, utilized a 2′,3′-dideoxy-DNA (ddD_n), identical in sequence to the DNAs above. DNAs were dissolved in 10 mM KCl and stored at −20 °C. Because of their extensive secondary structure, DNA concentrations were determined by UV/vis spectroscopy after complete digestion with P1 nuclease using the ε_{260} calculated from their constituent deoxyribonucleotides. dAMPCPP was purchased from Jena Bioscience (Jena, Germany).

Stopped Flow Kinetic Assays. Stopped flow experiments were performed on an Applied Photophysics (Leatherhead, U.K.) SX20 stopped flow apparatus having a dead time of 1.3 ms. For 2AP fluorescence, the excitation wavelength was 312 nm, the spectral bandpass was 4 nm, and fluorescence emission was measured using a 360 nm cutoff filter (Corion). For Trp-fluorescence, the excitation wavelength was 295 nm, the spectral bandpass was 4 nm, and emission was measured using a 320 nm cutoff filter (Corion).

Stopped flow fluorescence assays were performed at 37 °C in 50 mM each bisTris/AMPSO buffer, adjusted to a specific pH (range 6.1−8.9; see text). The ionic strength of the buffer was adjusted using KCl to the equivalent of 100 mM KCl as determined by ion conductivity measurement. Buffers also contained 30.4% glycerol (w/w), 1 mM DTT, and $MgCl_2$ [0−20 mM], as indicated in the text. In single turnover nucleotide (dT:dATP) incorporation (i.e., nucleotidyl transfer) experiments, solution A (0.5 μM Pol β; all concentrations are postmixing) was combined with solution B (0.2 μM DNA and a variable concentration of $Mg{\cdot}dATP^{2-}$ in the range 2.4−600 μM). In our previous studies,[19,35] Pol β kinetic experiments were performed by premixing polymerase and DNA and then initiating the reaction by addition of dNTP. Using that

method, much of the data pertaining to fast subdomain motion (k_{obs} = 10^2–10^3 s^{-1}) is lost during the ~4 ms of instrument dead time and mixing. The method employed in this study, whereby enzyme was mixed with a solution containing both DNA and dNTP, imposes a kinetic lag phase (~6 ms) due to DNA binding prior to dNTP-induced subdomain motion, which enables observation of the entire kinetic phase covering the conformational step.

Sequential-mixing stopped flow experiments to measure the kinetics of the reverse pathway upon quenching of the reaction with EDTA were performed similarly as before.[36] In these experiments, solution A (0.5 μM Pol β) was initially mixed with solution B (0.2 μM DNA and 131 μM Mg·dATP^{2-}), both with 0.2 mM Mg^{2+}, and allowed to age for 15 ms, during which time transient enzyme intermediates accumulate. After this aging time, the reaction was mixed with solution C (buffer which included 20 mM EDTA and no $MgCl_2$).

Stopped flow absorbance assays were performed in weakly buffered solutions in the presence of pH indicator comprised of either 0.5 mM MES/0.05 mM bromocresol purple (pH 6.2) or 0.5 mM bicine/0.05 mM cresol red (pH 8.6). Solutions also included 100 mM KCl, 1 mM DTT, and 30.4% glycerol. Dissolved CO_2 was removed from stock solutions of buffer/indicator by N_2 sparging, and reaction solutions were prepared using vacuum degassed H_2O. For these measurements and the supporting intrinsic Trp fluorescence measurements, solution A (9.2 μM of Pol β, *no indicator*) was combined with solution B (8.5 μM DNA, 100 μM Mg·dATP^{2-}, and indicator); the final concentration of indicator was 0.05 mM after mixing. The solutions also contained a variable concentration of $MgCl_2$ (indicated in the text). Proton binding by the pH indicator was monitored by absorbance at 590 nm (bromocresol purple) or 574 nm (cresol red), and proton equivalents were calculated from specific color changes determined in separate calibration experiments using standard solutions of HCl.

Rapid Chemical Quench Assays. Single turnover experiments (37 °C in bisTris/AMPSO buffer, pH 6.2 or 6.8, identical to those described above) were done using a KinTek (Austin, TX) RQF-3 instrument. Reactions were performed by combining a solution containing (final concentrations) 2 μM Pol β with a solution containing 1 μM DNA and 100 μM Mg·[α-^{32}P]-dATP^{2-} (>98% saturating); both solutions contained a variable concentration of Mg^{2+} (0.07–20 mM). The reactions were quenched using 0.2 M EDTA. The reaction was followed by the incorporation of [α-^{32}P]-dAMP in the DNA by acid precipitation. Briefly, an aliquot of each sample was transferred to a tube containing 10 μL of 50 μM carrier DNA (random oligos approximately 50–100 nucleotides in length) and 1 mg/mL BSA and precipitated with 750 μL of 15% cold trichloroacetic acid (TCA). The DNA was precipitated by centrifugation (12000*g*, 20 min) and then washed several times with cold 15% TCA. The precipitates were dissolved in 10 mM NaOH and 0.1% SDS, and the radioactivity was measured by liquid scintillation counting. The total radioactivity (per volume) in the original RQF sample before precipitation was also determined and used to calculate the normalized amount of radioactivity incorporated into the DNA.

Conventional Data Analysis. Nonlinear regression analysis was performed by the program gnuplot (http://www.gnuplot.info/). Both stopped flow and rapid quench kinetic traces were analyzed according to eq 1, where where A is the total amplitude change, t is time in seconds, λ is the rate term (which approximates the observed k_{pol}), and C is a baseline term. [Note: For stopped flow traces, only the portion of the curve corresponding to the slow, rate-limiting portion of the reaction was analyzed. For rapid quench experiments, the normalized radioactivity incorporated, $f(t)$, divided by A is equal to the fraction of product D_{n+1} formed.]

$$f(t) = A(1 - e^{-t\lambda}) + C \quad (1)$$

To determine pH-dependent rate constants (k_{pol}) and Mg^{2+} dissociation constants (K_d^{Mg}), observed rate constants (k_{obs}) were analyzed as a function of [Mg^{2+}] according to eq 2a or, in cases where substrate-like inhibition by Mg^{2+} was observed, eq 2b:

$$k_{pol(app)} = \frac{k_{pol}[Mg]}{[Mg] + K_d^{Mg}} \quad (2a)$$

$$k_{pol(app)} = \frac{k_{pol}[Mg]}{[Mg] + K_d^{Mg} + \frac{[Mg]^2}{K_{II}}} \quad (2b)$$

Global Analysis of Kinetic Data. Global kinetic analysis was performed using KinTek Explorer and FitSpace Explorer.[37,38] The following strategy was used to collect stopped flow fluorescence data for Pol β intended for global analysis: (i) First, background fluorescence of buffer, free Pol β, and free DNA were measured under the same conditions (pH, temperature, etc.) as the kinetic assays. (ii) The kinetics of Pol β·DNA (ED_n) binary complex formation was independently measured to determine amplitudes and rate constants involved in the formation of the ED_n complex and other intermediates. (iii) Finally, stopped flow fluorescence assays to measure nucleotidyl transfer were performed. A complete description of DNA-binding kinetics and further details pertaining to analysis of kinetic data are provided as Supporting Information.

Complex Formation of Mg^{2+} with dATP and Tri(poly)-phosphate. The equilibrium concentrations of Mg·dATP^{2-} (or Mg·PPP_i^{2-}) and Mg^{2+} in experiments were computed using literature values of the pK_a and Mg^{2+} dissociation constants for Mg·dATP^{2-} (28 μM) and Mg_2·dATP^0 (25.1 mM),[39] and these calculations are provided in the Supporting Information. For tri(poly)phosphate, the active form is presumed to be Mg·X·PPP_i^{2-}, where X = Na^+, K^+, or H^+; binding of X was not considered in the calculation.

RESULTS AND ANALYSIS

Pol β Stopped Flow Fluorescence Kinetics. Pre-steady-state kinetic experiments measuring single nucleotide incorporation catalyzed by Pol β were performed at 37 °C, pH 7.1, over a range of both [Mg^{2+}] and [Mg·dATP^{2-}]. As described previously, the stopped flow kinetics of Pol β-catalyzed nucleotidyl transfer monitored by fluorescence using either intrinsic Trp or 2AP-labeled DNA is dominated by two phases that correspond to large-scale subdomain motions that occur during catalysis.[19,35] The rapid fluorescence increase seen at early time points corresponds to the subdomain open-to-close transition induced upon nucleotide (Mg·dNTP^{2-}) binding. The subsequent decrease in fluorescence corresponds to subdomain reopening after nucleotidyl transfer (i.e., chemistry), and the rate of this step has been shown by us to be limited by chemistry under these conditions.[35] All the data together were analyzed globally using KinTek Explorer[37,38] according to two alternative models for nucleotide induced subdomain motion involving either one or two conformational steps. The results

Table 1. Kinetics of dT:dATP Insertion by Pol β[a]

		one-step	two-step
K_d^{dATP} $(1/K_1)$	μM	300[b]	724[b]
$k_{+2(a)}$	s^{-1}	1365 ± 155	3190[c]
$k_{-2(a)}$	s^{-1}	11.9 ± 2.8	32.1[c]
$k_{+2(b)}$	s^{-1}		122[c]
$k_{-2(b)}$	s^{-1}		11.6[c]
K_d^{Mg} $(1/K_3)$	mM	1.76 ± 0.38	1.56 ± 0.30
k_{+4}	s^{-1}	6.43 ± 1.15	6.38 ± 0.93
(ED)		1[b]	1[b]
(EDN)		1.83[d]	2.26[d]
(E′DNM)		2.47 ± 0.03	2.46 ± 0.01
χ^2/ndf		82.8	77.6

[a]Kinetic parameters were derived by global fitting to Scheme 1 or an analogous scheme having two conformational steps [2a and 2b]. Kinetic and binding parameters for steps 2−4 and fluorescence amplitude parameters (relative units) for ED, EDN, and E′DNM species are reported. Error limits were derived from contour confidence analysis (Figure 3) reflecting values within 1.2× the chi squared (χ^2/ndf) minimum. [b]Value fixed during global fit. [c]Lower limit defined only. [d]Upper limit defined only.

from both analyses are shown in Table 1, and the best fit results to the two-step model are shown in Figure 2. Complete details describing the mechanisms used in global analysis are provided as Supporting Information. Particular aspects of the evaluated models are described below.

Kinetics of Nucleotide-Induced Subdomain Closing. The conventional, one-step conformational model is described in Scheme 1. In the two-step model, step 2 is divided into {EDN ⇌ E_iDN ⇌ E′DN}, steps 2a and 2b, respectively, where E_iDN is a partially closed intermediate complex. On the basis of the relative chi squared (χ^2/ndf) for each fit, the data were better described by the two-step (χ^2/ndf = 77.6) than by the one-step subdomain closing mechanism (χ^2/ndf = 82.8). The information content of the data pertaining to subdomain motion is unfortunately limited both by the very rapid kinetics and because the proposed intermediate in the two-step mechanism, E_iDN, is not predicted to accumulate in the pre-steady state; thus, the conclusion of biphasic subdomain motion should be considered tentative. In the two-step mechanism, a very rapid (10^3−10^4 s^{-1}) conformational change occurs upon nucleotide binding, followed by a slower (10^1−10^2 s^{-1}) relaxation that results in full subdomain closing. Both models were evaluated by confidence contour analysis (Figure 3) as described by Johnson et al.,[38] which indicated that the one-step mechanism is well determined, while only lower limits can be determined for rates pertaining to biphasic conformational closure [steps 2a and 2b].

Kinetics of Mg·dATP^{2-} Binding. Global analysis of the one-step conformational change mechanism yielded a lower limit for K_d^{dATP} on the order of 10−100 μM and of the two-step mechanism, a K_d^{dATP} on the order of 100 μM−1 mM (Table 1). This difference can be rationalized in that the two-step mechanism explicitly accounts for very rapid and exothermic isomerization of the EDN complex [step 2a] to form the intermediate, EDN_i, whereas the one-step mechanism does not. The $K_{d(app)}$ for Mg·dATP^{2-} (~2.7 ± μM), defined here as $1/(K_1K_2)$ or $1/(K_1K_{2a}K_{2b})$, is similar for both models and consistent with a value (1.2 μM) determined in an independent titration experiments measuring the equilibrium binding of Mg·dATP^{2-} to form a closed ternary complex with Pol β and 2′,3′-dideoxy-DNA (Figure 4A).

We reasoned that initial binding of dNTP is dominated by interactions involving the Mg−triphosphate moiety with the enzyme; this is consistent with structure−function studies of Pol β.[15,40] We therefore performed a titration of the E·D_n complex with Mg·tri(poly)phosphate, Mg·PPP_i (Figure 4B). Interestingly, there was a small fluorescence increase upon Mg·PPP_i binding, suggesting that the E·D_n·Mg·PPP_i complex is partially closed. Analysis of the titration yielded a K_d for

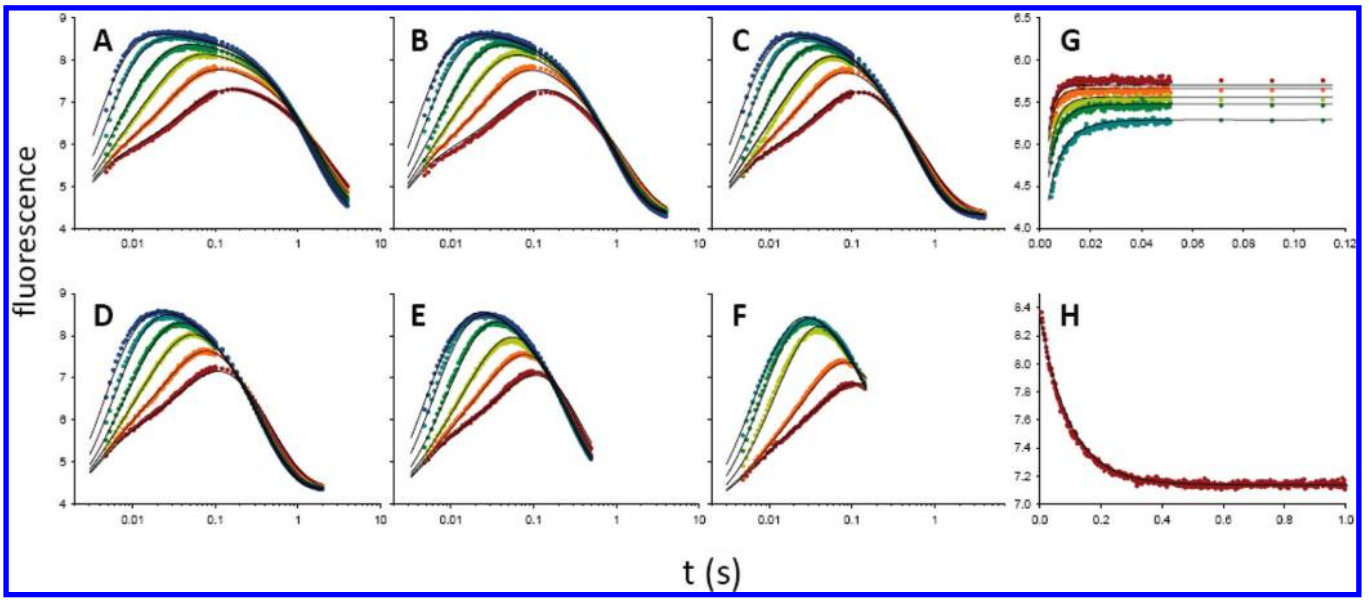

Figure 2. Global analysis of stopped flow fluorescence kinetic data. In all experiments, Pol β was 500 nM and DNA was 200 nM. (A−F) Single turnover nucleotidyl transfer reactions: dT:dATP insertion (plotted on a log time scale). The solid lines are simulated results after global fit to the mechanism involving biphasic subdomain motion. In each panel, the curves are reactions performed at different [Mg·dATP^{2-}] in the range of 3−350 μM (red to blue). Each panel shows reaction sets performed at a given [Mg^{2+}]: (A) 0.2, (B) 0.4, (C) 0.75, (D) 1.5, (E) 2.5, and (F) 5.0 mM. (G) Stopped flow kinetics of ED_n binary complex formation. The solid lines show simulated result after global fit to *only* the DNA binding portion of the mechanism. (H) Kinetics of subdomain reverse opening; [Mg^{2+}] after first mix was 0.2 mM (trace after second mix with EDTA is shown).

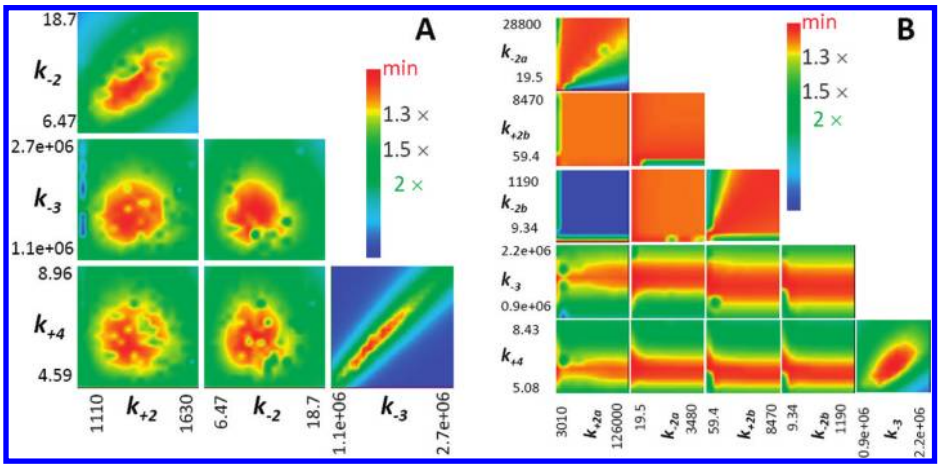

Figure 3. Confidence contour analysis. FitSpace Explorer[38] was used to determine upper and lower boundaries of the indicated rate constants for mechanisms involving (A) one- and (B) two-step subdomain conformational change. In this analysis, amplitude terms are held constant, each rate constant is varied and held constant in pairs, and all other rate constants are refit by global analysis. The ratio of the resulting χ^2/ndf value to that of the original best-fit solution is calculated and used to generate the contour plots; the red zone defines a region of good fit corresponding to maximum deviation of 20% (1.2×) in χ^2/ndf value. For the two-step mechanism (B), confidence analysis reveals that the upper limits for the rates of subdomain conformational steps (2a and 2b) are not defined.

Mg·PPP$_i$ of 280 μM, similar to the estimates of K_d^{dATP} from global analysis of nucleotidyl transfer kinetic data (Table S2). The results support that weak initial nucleotide binding, primarily mediated by Mg^{2+}–triphosphate interactions, is followed by an energetically favorable conformational closing step upon recognition of a correct base pair.

Kinetics of Mg^{2+} Binding and Chemistry and Evaluation of a "Prechemistry" Step by Kinetic Simulation. The kinetic data are consistent with a mechanism involving the rapid equilibrium binding of Mg^{2+} [Scheme 1, step 3], followed by a single rate-determining step for nucleotide insertion chemistry [step 4]. Analysis using both one- and two-step conformational mechanisms (Table 1) gave essentially identical solutions for k_{pol} (~6.4 s^{-1}) and K_d^{Mg} (~1.7 mM). Others have proposed mechanisms that involve an additional kinetic step before chemistry.[23,24,33] To investigate this mechanism by kinetic simulation, we deliberately constructed a more complex mechanism that includes a prechemistry step: the isomerization of E′DNM to form an activated enzyme complex, E″DNM (Figure 5A). The purpose of the simulation was to determine if the kinetic data are consistent with such a mechanism and to investigate quantitatively how the rate constants for the prechemistry and chemistry steps can vary, given the constraints imposed by the data, thus providing insight into possible mechanisms.

Here we considered a general case (Figure 5A) where step 1′ is reversible and step 2′ is irreversible. Only the rate constants involved in Mg^{2+} binding, steps 1′ and 2′, and the amplitude terms for E′DNM and E″DNM (which were constrained to be equal) were fit, and all other parameters were held constant at their best fit values. Since we are interested in mechanisms that include two rate-determining steps, we constrained the forward rate constants, k_1' and k_2', at various fixed ratios between 0.01 and 100 and then refit the experiment; the best-fitted parameters are reported in Figure 5B. This analysis shows there are multiple solutions to the prechemistry model that satisfy the data, indicating, as expected, that the data contain insufficient information to determine a prechemistry step. Figure 5B demonstrates that as the k_1':k_2' ratio varies between 0.1 and 10, k_{-1}' is optimized so that the overall flux through both steps can account for the observed rate of nucleotide insertion (k_{pol}). Note at the extreme ends of the x-axis two situations occur, both of which represent kinetic collapse of the mechanism to a single rate-limiting step. When $k_1' \ll k_2'$, the K_1' equilibrium is unfavorable, but a very fast and exothermic step 2′ drives the reaction forward. In this situation, the observed rate (k_{pol}) establishes a lower limit for k_1'. When $k_1' \gg k_2'$, the equilibrium steps K_d^{Mg} and K_1' become linked, and the value for K_d^{Mg} increases to compensate for a very fast and exothermic step 1′. In this situation, the observed rate (k_{pol}) establishes a lower limit for k_2'. Interestingly, when both steps 1 and 2 are made irreversible (Supporting Information, Figure S5), the simulation indicates a poor fit when $k_1' \geq k_2'$, indicating that a mechanism with two irreversible rate-determining steps is not supported by the data. Overall, the simulations demonstrate that a reversible, nonequilibrium prechemistry step is consistent with kinetic data.

pH- and [Mg^{2+}]-Dependence Studies. Proper active site assembly is a prerequisite for enzyme catalysis,[41] and for DNA polymerases, this entails Mg^{2+} binding and subsequent structural reorganization around the metal, including proton transfer.[25,27,28] The kinetics and mechanism of this process is poorly understood; thus, we performed additional kinetic studies. In a pH range of (6.2–8.9), the observed rate of nucleotidyl transfer (k_{obs}) was plotted against [Mg^{2+}] to determine apparent (pH-dependent) K_d^{Mg} and k_{pol} values (Supporting Information, Figure S6A,B; replots for pH 6.2 and 8.6 are also shown in Figure 7C,D for comparison to rapid quench results, described below). At pH > 8, inhibition at high [Mg^{2+}] was evident; this was analyzed by an uncompetitive inhibition model to extract K_d^{Mg} and k_{pol} values (Supporting Information, Figure S6C). Figure 6 shows the pH dependence of pK_d^{Mg} and log(k_{pol}). The pK_d^{Mg} varies between two limiting values, with stronger binding at high pH (Figure 6A), consistent with a one-proton binding/dissociation event. The S-shape of the curve indicates that Mg^{2+} is capable of binding to a protonated form of the active site with lower affinity. Therefore, the data were analyzed according to eq 3. Limiting values (Y_{limit}) for K_d^{Mg} are 37.5 and 0.32 mM at low and high pH conditions, respectively. The macroscopic pK_a value of 7.13

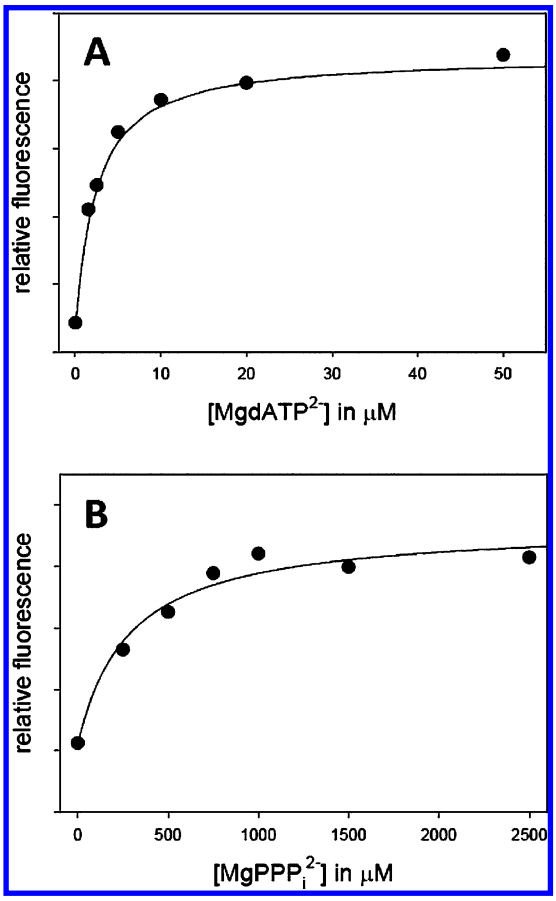

Figure 4. Equilibrium binding of Mg·dATP^{2-} and Mg·tri(poly)-phosphate to the Pol β–DNA complex. Conditions were pH 7.1, 0.2 mM $MgCl_2$, 37 °C. Pol β and DNA concentrations were 500 and ~200 nM, respectively. The solid curve shows the best fit to the binding equation: $f(x) = a[L]/(K_d + [L]) + bkg$, where a is the amplitude change, L is the ligand (Mg·dATP^{2-} or Mg·tri(poly)phosphate), K_d is an apparent binding constant, and bkg is the fluorescence of the enzyme–DNA complex without added ligand. Solutions for K_d were (A) 1.2 μM (Mg·dATP^{2-}) and (B) 281 μM (Mg·tri(poly)-phosphate).

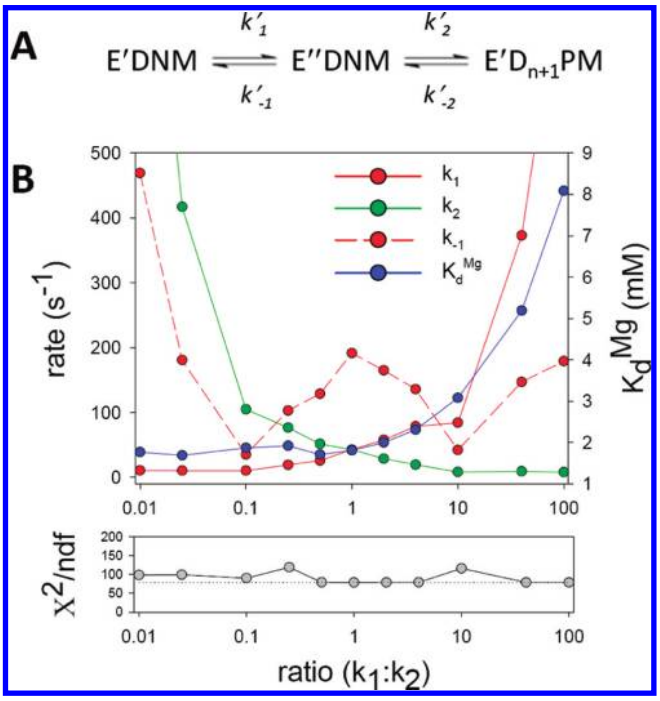

Figure 5. Kinetic simulation of a hypothetical prechemistry step. (A) Simulated kinetic model involving prechemistry isomerization [1′] and chemistry [2′] steps. (B) The fitted parameters k_1', k_{-1}', k_2', and K_d^{Mg} from multiple global fits of the data (same data set as in Figure 2) and the corresponding χ^2/ndf values are plotted versus the ratios of k_1':k_{-1}', as described in the text; k_{-2}' was held constant at zero. The dotted reference line in (B) indicates the minimum χ^2/ndf from the original data fit.

(Figure 6A) corresponds to ionization of E′DN (i.e., the enzyme form that binds Mg^{2+}).

$$pK_d^{Mg} = \frac{Y_{limit1} + (Y_{limit2} \times 10^{pK_a - pH})}{1 + 10^{pK_a - pH}} \quad (3)$$

Our data demonstrate an increase in k_{pol} at high pH (Figure 6B), similar to previous pH dependence studies of Pol β.[20,22] This is consistent with general base catalysis involved in the formation of the 3′-O$^-$ nucleophile on the enzyme. However, the pH dependence of log(k_{pol}) does not conform to a simple Henderson–Hasselbalch description, but instead increases gradually over at least 3 pH units with a Hill parameter of 0.47 (slope in the log–log plot, Figure 6B). This type of irregular pH titration is often an indication of an electrostatic interaction (cooperativity) between two or more protonic groups involved in catalysis.[42,43] Alternatively, as Cleland notes in his classical work,[44] a flat pH–rate profile could result if proton dissociation from the Michaelis complex [{E′D$_n$NM·H$^+$ ⇌ E′D$_n$NM + H$^+$}; pK_a = 5.56, calculated from the pK_a of E′D$_n$N (7.13) and the two limiting K_d^{Mg} values, Figure 6A] is slow relative to substrate dissociation and the central step (chemistry). Because of the limited pH range accessible by experiment, as well as the irregular pH–rate profile, the maximum k_{pol} and the associated apparent pK_a value could not be defined. This conclusion differs substantially from previous studies,[20,22] although the general pH trend is consistent (see Supporting Information).

To corroborate the results obtained by the stopped flow experiments (above) and to further investigate the observed uncompetitive inhibition by Mg^{2+}, additional rapid quench experiments were performed to directly measure the rate of nucleotidyl transfer as a function of [Mg^{2+}] at pH 6.2 and 8.6. Figure 7A,B shows the time courses of product D$_{n+1}$ formation at pH 6.2 and 8.6, respectively, and these data were analyzed by nonlinear regression (eq 1) to obtain observed rate constants (k_{obs}). The replots (k_{obs} versus [Mg^{2+}]) are shown in Figure 7C,D and compared with those from stopped flow studies (described above) performed under identical pH conditions. At pH 6.2 (Figure 7C), there is excellent agreement between the results obtained by the two methods, supporting the previous conclusion[20] that chemistry is overall rate limiting at low pH. At pH 8.6 (Figure 7D), the inhibition observed at high [Mg^{2+}] in the stopped flow experiment is not observed in the rapid quench experiment. This indicates that the inhibition is not due to enzyme inactivation, but instead due to the decrease in rate of a step after chemistry. Note the results obtained by analysis of the stopped flow data accurately predict the results of the rapid quench experiment—absent uncompetitive inhibition (Figure 7D, dotted line). This difference seen in k_{pol} values obtained by the two assay methods at high pH has previously been attributed to a pH-dependent increase in the rate of chemistry such that a later step (most likely subdomain

dx.doi.org/10.1021/bi200954r | Biochemistry 2011, 50, 9865–9875

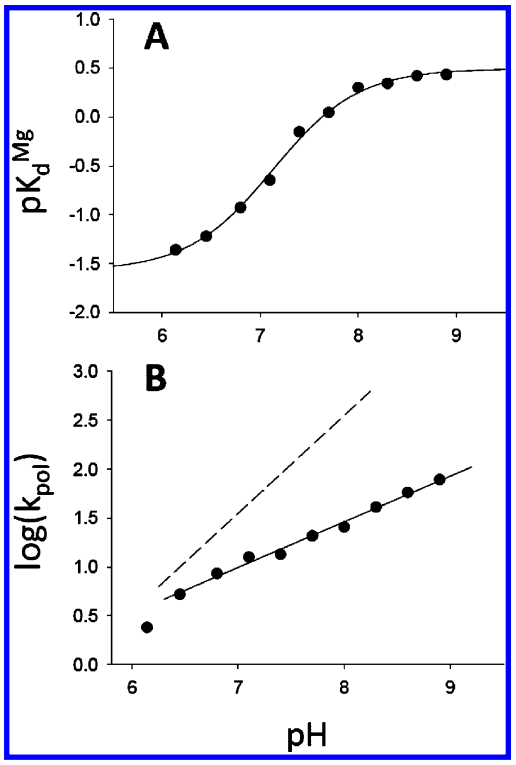

Figure 6. pH dependence of kinetic parameters of Pol β. (A) Variance of pK_d^{Mg} (K_d in mM) as a function of pH. (B) Variance of $\log(k_{pol})$ (k_{pol} in s^{-1}) with pH. The solid line shows the linear regression fit of the data between pH 6.4 and 8.9. The slope defines the Hill parameter (0.47); an arbitrary line (dashed) with slope = 1 is shown for reference.

opening after chemistry) becomes rate limiting.[20] According to Scheme 1, subdomain opening after chemistry [step 6] occurs after Mg^{2+} dissociation from the enzyme [step 5]; thus, we conclude that Mg^{2+} inhibition is attributed to accumulation of the intermediate, E′D_{n+1}PM, resulting in a decrease in the rate of flux through these two steps.

Stopped Flow Absorption Kinetics of Enzymatic Proton Generation. The following experiments were performed to measure the kinetics and stoichiometry of proton release during enzyme catalysis. The formation of protons was detected by absorption change of the pH indicator present in the reaction solution. In Figure 8, the absorbance data are superimposed by data from stopped flow experiments measuring intrinsic Trp fluorescence performed under identical conditions. The results show that at pH 6.2 (Figure 8A) the rate of H^+ formation is coincidental with k_{pol} (1.0 ± 0.1 s^{-1}). Under this condition, subdomain opening [step 6], which is reported by the change in Trp fluorescence, is fast relative to chemistry. At higher pH, the rate of the chemical step increases. At pH 8.6 (Figure 8B), the rate of H^+ formation (70 s^{-1}) is approximately 4-fold faster than the Trp fluorescence change (17 s^{-1}). It is remarkable that at high pH proton release occurs prior to subdomain opening [step 6]. This result indicates, in accordance with microscopic reversibility, that the reverse reaction (pyrophosphorolysis) can occur by binding of a proton to the closed E′D_{n+1}PM complex.

The rate of proton formation corresponds either to formation of the 3′-O^- nucleophile in the active site or, alternatively, to deprotonation of the catalytic base prior to proton abstraction from 3′-OH. It is interesting to compare this

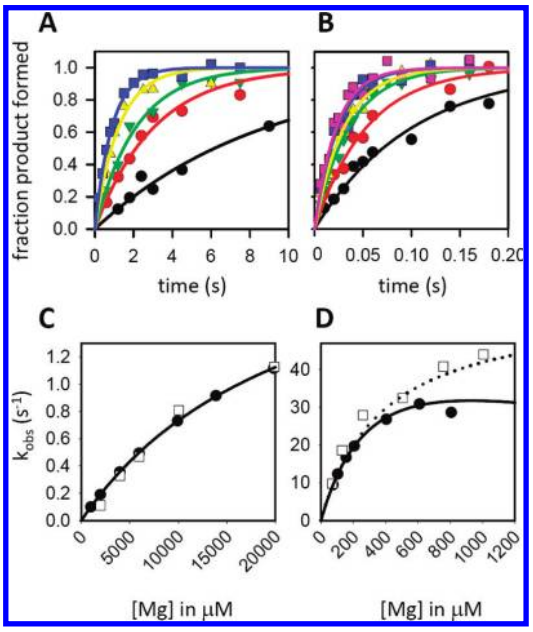

Figure 7. Rapid quench kinetics of Pol β and comparison to stopped flow results. Reaction time courses are shown for experiments performed at (A) pH 6.2, [Mg^{2+}] = (ascending order) 1990, 4003, 5980, 10 060, and 19 920 μM and (B) pH 8.6, [Mg^{2+}] = 70, 132, 261, 506, 757, and 1006 μM. All experiments were performed at 37 °C. The solid curves (A, B) are individual fits of each data set to eq 1, and the replots of k_{obs} as a function of [Mg^{2+}] are shown in (C) pH 6.2 and (D) pH 8.6; the results from stopped flow (●) and rapid quench (□) experiments are plotted together for comparison. The solid curves (C, D) are best fits of the stopped flow data to eqs 2a and 2b, respectively. At pH 6.2 (C), k_{pol} = 2.41 s^{-1} and K_d^{Mg} = 22.8 mM. At pH 8.6 (D), k_{pol} = 57.86 s^{-1}, K_d^{Mg} = 0.38 mM, and K_{II}^{Mg} (uncompetitive inhibition constant) = 2.25 mM; the dotted curve is the same solution, only in the absence of Mg inhibition (eq 2a).

rate (70 s^{-1}) at pH 8.6 with the rate of nucleotidyl transfer (dotted line, Figure 7D) at this condition (~30 s^{-1}). These data suggest that deprotonation of the 3′-OH is a rate-determining step in the overall nucleotide insertion reaction. It is often assumed that deprotonation of the 3′-OH occurs as a concerted step with nucleotidyl transfer. However, our data suggest an alternative sequential mechanism involving two discrete *rate determining* steps—here, (i) 3′-OH deprotonation and (ii) nucleotidyl transfer. This mechanism predicts, similar to the results presented here (Figures 8A and 7D), that the *observed rate* of proton formation would be faster than that of the final product (D_{n+1}), given identical rates of the two microscopic rate steps (kinetic simulation, Figure S7; also see ref 45).

DISCUSSION

We combined pre-steady-state kinetics, [Mg]- and pH-variation studies, and kinetic simulation in an effort to characterize transient enzyme intermediates important in the Pol β reaction pathway. Our particular interest is in possible conformational steps that constitute prechemistry organization of the active site, including local conformational steps related to Mg binding and proton transfer. We report several major conclusions. First, we show that the kinetic mechanism of Pol β is adequately described with a single rate-limiting step corresponding to nucleotidyl transfer but that a rate-determining prechemistry step *is possible* given the constraints defined in our simulation

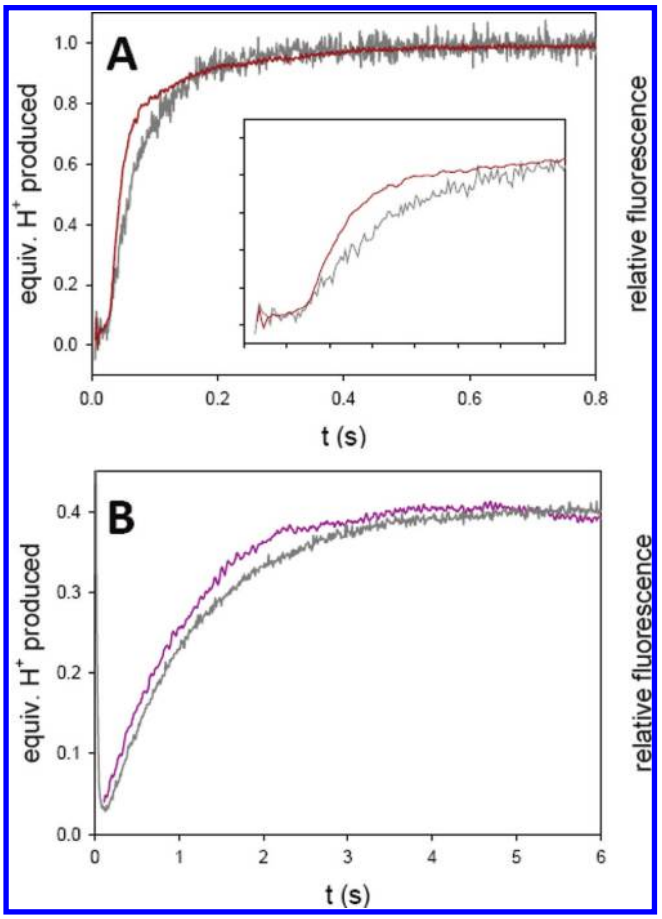

Figure 8. Stopped flow absorbance kinetics of enzymatic H^+-formation. Equivalents of H^+ produced by Pol β, colored, were determined from stopped flow absorbance traces. The stopped flow (intrinsic Trp-) fluorescence traces, gray, were normalized and scaled for superimposition. (A) Bicine, cresol red, pH 8.6, 0.5 mM $MgCl_2$: the Trp-fluorescence emission trace exhibits a single-component exponential change in fluorescence (λ = 17.4 s^{-1}) following a ~20 ms lag time that corresponds to formation of a closed E′DN ternary complex. The H^+-formation kinetic plot, red, is biphasic, dominated by a large amplitude phase (λ = 70.5 s^{-1}). A replot between 0 and 0.15 s is shown in the inset. (B) MES, bromocresol purple, pH 6.2, 20 mM $MgCl_2$: both Trp-fluorescence and H^+-formation plots exhibit single-component exponential kinetics with similar rates (λ = 0.90 and 1.10 s^{-1}, respectively). The observation of less than 1 equiv of protons formed can be explained by either formation of $H{\cdot}Mg{\cdot}PP_i^{1-}$ or by net proton binding to the product ($E{\cdot}D_{n+1}$) enzyme species.

study. We provide evidence to support that proton abstraction from the 3′-OH is rate determining for single nucleotide incorporation. A recent computational study proposed that proton transfer occurs concertedly with rate limiting nucleophilic attack.[25] Our observation that proton release occurs faster than nucleotidyl transfer (at pH 8.6) seems to be in conflict with a strictly concerted mechanism. Lin et al.[24] alternatively proposed that the deprotonation of the 3′-OH occurs as an equilibrium step, prior to the formation of a transient enzyme intermediate in which the Mg-coordinated 3′-O^- is poised for nucleophilic attack on the αP. Our data are consistent with this mechanism but further suggest that the rate of proton transfer from 3′-OH is similar to that of nucleotidyl transfer.

It has long been understood that binding of a correct dNTP induces a conformational change in DNA polymerases that activates the enzyme for nucleotidyl transfer.[7,14] Here we present experimental evidence in support of two discrete steps in the nucleotide-induced subdomain closing of Pol β. Our data, of course, do not address the structural mechanism of this conformational change. Previously, however, computational studies from the Schlick laboratory[25] suggested that subdomain closing occurs by a biphasic process involving the sequential rearrangement of side chains D192, R258, and F272. It was proposed that a steric clash between R258 and F272 delays the enzyme in a partially open conformation. Mutation studies with R258A Pol β indicated that R258 does not impede the forward reaction rate but that subdomain opening in the reverse direction was faster for the mutant.[20,36] This is consistent with R258 forming a stabilizing interaction in the closed ternary complex.

It has been proposed that having multiple kinetic steps prior to chemistry could affect polymerase fidelity by imposing so-called "kinetic checkpoints".[46−48] These proposed steps include both nucleotide-induced global conformational changes and more subtle conformational changes associated with the preparation of the active site for chemical catalysis. While structural[49] and computational studies[23,50] have given insight into the molecular mechanisms for coupling substrate binding and recognition with enzyme activation, the impact of these individual steps on the kinetics of correct versus incorrect dNTP incorporation (and, hence, fidelity) is controversial. It has been pointed out that multiple prechemistry steps would not be expected to affect fidelity, provided that these steps occur faster than the rate-limiting chemical step.[26,51] Our data are consistent with this idea, showing that formation of an active E′DNM complex (for Pol β) occurs essentially as a rapid equilibrium step. Moreover, binding of an incorrect dNTP is known to destabilize the closed enzyme conformation leading to infrequent formation or malformation of the active site, resulting in inefficient catalysis. Together, these data support that ground-state dNTP binding and equilibration of subsequent conformational steps are important for polymerase fidelity: for correct dNTP binding, these steps are favorable, allowing for efficient catalysis, whereas for incorrect dNTP binding, these steps are unfavorable, allowing for facile dNTP dissociation rather than chemistry, consistent with a large body of structural[14,15,28,49] and experimental[29,52−54] studies.

The mechanism of general base and general acid catalysis in enzyme-catalyzed nucleotidyl transfer is a subject of intense interest. Proton migration within the active site would logically be expected to stabilize negative charge that develops at the transition state of nucleotidyl transfer.[8] The pH dependence of k_{pol} reported here supports a role for general base catalysis. In Pol β, the same residue—D256—has been implicated in both ground-state Mg^{2+}-binding and general base catalysis, and the observed pH dependence of pK_d^{Mg} and k_{pol} likely reflects ionization of this residue in the absence or presence of the bound Mg^{2+} ion, respectively. The pH dependence of k_{pol} is irregular, implicating multiple protonic groups involved in catalysis, and thus could reflect ionization of a separate group, perhaps an intervening species involved in proton transfer between the 3′-OH of DNA and bulk solvent (Figure 1). In general, the irregular pH dependence of an enzyme activity suggests electrostatic interaction between multiple protonic sites, a phenomenon which is now understood to be common for enzymes.[42,43,55] Electrostatic interactions in proteins can occur either directly (via Columbic interactions) or by conformational effects if the ionization of a residue structurally

alters the microenvironment (and thus the microscopic pK_a) of another group. In summary, our kinetic data in total support that deprotonation of the 3′-OH is a rate-determining step in the Pol β reaction. We propose this proton is transferred to other groups in the active site, thus providing important charge stabilization during catalysis. Finally, proton dissociation from the enzyme can occur prior to—and is possibly the event that triggers—subdomain opening [step 6] prior to release of products.

Our presented evidence for the involvement of multiple protonic groups in proton transfer and general base catalysis is in accordance with a number of recent studies. For example, independent computational studies[33,56] have proposed mechanisms that involve multiple, discrete proton transfer events between the 3′-OH, catalytic protein residues, and active site waters that are coupled to nucleotidyl transfer. Experimental studies of Pol β by Sucato et al.[21,22] provided evidence that pyrophosphate formation was rate determining for chemistry, and Castro et al.[57,58] concluded that multiple proton transfer events were involved in catalysis based on solvent deuterium kinetic isotope effects of several polymerases (not including Pol β). Our proposed model of electrostatic cooperativity provides a similar, but differently nuanced, explanation for their proton inventory study. Castro et al.[57,58] proposed that general acid catalysis was required to promote pyrophosphate elimination based on their evidence for a second protonic group and their pH-dependence studies. Our pH-dependence studies are consistent with proton transfer between the 3′-OH and multiple active site groups, including to the pyrophosphate leaving group. Our kinetic data are also consistent with a rate-determining step corresponding to pyrophosphate elimination and/or subsequent active site disassembly. We caution that there are substantial differences among residues that line the dNTP binding pockets of the active sites of DNA polymerases in general and between Family X and other DNA polymerase families in particular, which suggests the possibility of alternative pathways for proton transfer in different systems.

■ ASSOCIATED CONTENT

Supporting Information

Tables S1 and S2 providing complete solutions from global analysis to the kinetic mechanisms for ED binary complex formation and nucleotidyl transfer, respectively; Table S3 giving calculated concentrations of free Mg^{2+} and $Mg{\cdot}dATP^{2-}$ used in stopped flow studies; Figure S1 describing the exact kinetic models used in global analysis; Figures S2−S4 describing experiments characterizing the kinetics and mechanism of ED binary complex formation; Figure S5 describing additional kinetic simulations of the prechemistry step mechanism; Figure S6 describing details of the pH- and $[Mg^{2+}]$-dependence study, the results of which are reported in Figure 6; Figure S7 describing kinetic simulation of sequential proton transfer and nucleotidyl transfer steps; additional analytical methods. This material is available free of charge via the Internet at http://pubs.acs.org.

■ AUTHOR INFORMATION

Corresponding Author

*Phone: +886-2-2789-9363. Fax: +886-2-2788-9759. E-mail: mdtsai@gate.sinica.edu.tw.

Funding

This work was supported by funds from Academia Sinica.

■ ACKNOWLEDGMENTS

We thank Dr. Marina Bakhtina for critical reading of the manuscript. We also thank New England BioLabs (Ipswich, MA) for use of their RQF3 rapid quench instrument.

■ ABBREVIATIONS

Pol, DNA polymerase; ASFV, African swine fever virus; PP_i, inorganic pyrophosphate; PPP_i, inorganic tri(poly)phosphate); bisTris, 1,3-propanediol, 2-(bis(2-hydroxyethyl)amino)-2-(hydroxymethyl); AMPSO, *N*-(1,1-dimethyl-2-hydroxyethyl)-3-amino-2-hydroxypropanesulfonic acid; MES, 2-(*N*-morpholino)-ethanesulfonic acid; TCA, trichloroacetic acid; dAMPCPP, 2′-deoxyriboadenosine-5′-[α,β-methylene] triphosphate.

■ REFERENCES

(1) Kunkel, T. A., and Bebenek, K. (1988) Recent studies of the fidelity of DNA synthesis. *Biochim. Biophys. Acta 951*, 1−15.
(2) Kunkel, T. A., and Bebenek, K. (2000) DNA replication fidelity. *Annu. Rev. Biochem. 69*, 497−529.
(3) Singhal, R. K., and Wilson, S. H. (1993) Short gap-filling synthesis by DNA polymerase beta is processive. *J. Biol. Chem. 268*, 15906−15911.
(4) Weissbach, A. (1979) The functional roles of mammalian DNA polymerase. *Arch. Biochem. Biophys. 198*, 386−396.
(5) Starcevic, D., Dalal, S., and Sweasy, J. B. (2004) Is there a link between DNA polymerase beta and cancer? *Cell Cycle 3*, 998−1001.
(6) Aravind, L., and Koonin, E. (1999) DNA polymerase β-like nucleotidyltransferase superfamily: Identification of three new families, classification and evolutionary history. *Nucleic Acids Res. 27*, 1609−1618.
(7) Steitz, T. A., Smerdon, S. J., Jager, J., and Joyce, C. M. (1994) A unified polymerase mechanism for nonhomologous DNA and RNA polymerases. *Science 266*, 2022−2025.
(8) Steitz, T. A., and Steitz, J. A. (1993) A general two-metal-ion mechanism for catalytic RNA. *Proc. Natl. Acad. Sci. U. S. A. 90*, 6498−6502.
(9) Dahlberg, M. E., and Benkovic, S. J. (1991) Kinetic mechanism of DNA polymerase I (Klenow fragment): identification of a second conformational change and evaluation of the internal equilibrium constant. *Biochemistry 30*, 4835−4843.
(10) Kuchta, R. D., Benkovic, P., and Benkovic, S. J. (1988) Kinetic mechanism whereby DNA polymerase I (Klenow) replicates DNA with high fidelity. *Biochemistry 27*, 6716−6725.
(11) Vande Berg, B. J., Beard, W. A., and Wilson, S. H. (2001) DNA structure and aspartate 276 influence nucleotide binding to human DNA polymerase beta. Implication for the identity of the rate-limiting conformational change. *J. Biol. Chem. 276*, 3408−3416.
(12) Wong, I., Patel, S. S., and Johnson, K. A. (1991) An induced-fit kinetic mechanism for DNA replication fidelity: direct measurement by single-turnover kinetics. *Biochemistry 30*, 526−537.
(13) Zhong, X., Patel, S. S., Werneburg, B. G., and Tsai, M. D. (1997) DNA polymerase beta: multiple conformational changes in the mechanism of catalysis. *Biochemistry 36*, 11891−11900.
(14) Doublie, S., Sawaya, M. R., and Ellenberger, T. (1999) An open and closed case for all polymerases. *Structure 7*, R31−35.
(15) Sawaya, M. R., Prasad, R., Wilson, S. H., Kraut, J., and Pelletier, H. (1997) Crystal structures of human DNA polymerase beta complexed with gapped and nicked DNA: evidence for an induced fit mechanism. *Biochemistry 36*, 11205−11215.
(16) Arndt, J. W., Gong, W., Zhong, X., Showalter, A. K., Liu, J., Dunlap, C. A., Lin, Z., Paxson, C., Tsai, M. D., and Chan, M. K. (2001) Insight into the catalytic mechanism of DNA polymerase beta: structures of intermediate complexes. *Biochemistry 40*, 5368−5375.

(17) Bose-Basu, B., DeRose, E. F., Kirby, T. W., Mueller, G. A., Beard, W. A., Wilson, S. H., and London, R. E. (2004) Dynamic characterization of a DNA repair enzyme: NMR studies of [methyl-13C]methionine-labeled DNA polymerase beta. *Biochemistry 43*, 8911−8922.
(18) Kim, S. J., Beard, W. A., Harvey, J., Shock, D. D., Knutson, J. R., and Wilson, S. H. (2003) Rapid segmental and subdomain motions of DNA polymerase beta. *J. Biol. Chem. 278*, 5072−5081.
(19) Bakhtina, M., Lee, S., Wang, Y., Dunlap, C., Lamarche, B., and Tsai, M. D. (2005) Use of viscogens, dNTPalphaS, and rhodium(III) as probes in stopped-flow experiments to obtain new evidence for the mechanism of catalysis by DNA polymerase beta. *Biochemistry 44*, 5177−5187.
(20) Bakhtina, M., Roettger, M. P., Kumar, S., and Tsai, M. D. (2007) A unified kinetic mechanism applicable to multiple DNA polymerases. *Biochemistry 46*, 5463−5472.
(21) Sucato, C. A., Upton, T. G., Kashemirov, B. A., Batra, V. K., Martinek, V., Xiang, Y., Beard, W. A., Pedersen, L. C., Wilson, S. H., McKenna, C. E., Florian, J., Warshel, A., and Goodman, M. F. (2007) Modifying the beta,gamma leaving-group bridging oxygen alters nucleotide incorporation efficiency, fidelity, and the catalytic mechanism of DNA polymerase beta. *Biochemistry 46*, 461−471.
(22) Sucato, C. A., Upton, T. G., Kashemirov, B. A., Osuna, J., Oertell, K., Beard, W. A., Wilson, S. H., Florian, J., Warshel, A., McKenna, C. E., and Goodman, M. F. (2008) DNA polymerase beta fidelity: halomethylene-modified leaving groups in pre-steady-state kinetic analysis reveal differences at the chemical transition state. *Biochemistry 47*, 870−879.
(23) Alberts, I. L., Wang, Y., and Schlick, T. (2007) DNA polymerase beta catalysis: are different mechanisms possible? *J. Am. Chem. Soc. 129*, 11100−11110.
(24) Lin, P., Pedersen, L. C., Batra, V. K., Beard, W. A., Wilson, S. H., and Pedersen, L. G. (2006) Energy analysis of chemistry for correct insertion by DNA polymerase beta. *Proc. Natl. Acad. Sci. U. S. A. 103*, 13294−13299.
(25) Radhakrishnan, R., Arora, K., Wang, Y., Beard, W. A., Wilson, S. H., and Schlick, T. (2006) Regulation of DNA repair fidelity by molecular checkpoints: "gates" in DNA polymerase beta's substrate selection. *Biochemistry 45*, 15142−15156.
(26) Rucker, R., Oelschlaeger, P., and Warshel, A. (2010) A binding free energy decomposition approach for accurate calculations of the fidelity of DNA polymerases. *Proteins 78*, 671−680.
(27) Xiang, Y., Oelschlaeger, P., Florian, J., Goodman, M. F., and Warshel, A. (2006) Simulating the effect of DNA polymerase mutations on transition-state energetics and fidelity: evaluating amino acid group contribution and allosteric coupling for ionized residues in human pol beta. *Biochemistry 45*, 7036−7048.
(28) Batra, V. K., Beard, W. A., Shock, D. D., Krahn, J. M., Pedersen, L. C., and Wilson, S. H. (2006) Magnesium-induced assembly of a complete DNA polymerase catalytic complex. *Structure 14*, 757−766.
(29) Tsai, Y. C., and Johnson, K. A. (2006) A new paradigm for DNA polymerase specificity. *Biochemistry 45*, 9675−9687.
(30) Florian, J., Goodman, M. F., and Warshel, A. (2003) Computer simulation of the chemical catalysis of DNA polymerases: discriminating between alternative nucleotide insertion mechanisms for T7 DNA polymerase. *J. Am. Chem. Soc. 125*, 8163−8177.
(31) Florian, J., Goodman, M. F., and Warshel, A. (2005) Computer simulations of protein functions: searching for the molecular origin of the replication fidelity of DNA polymerases. *Proc. Natl. Acad. Sci. U. S. A. 102*, 6819−6824.
(32) Radhakrishnan, R., and Schlick, T. (2005) Fidelity discrimination in DNA polymerase beta: differing closing profiles for a mismatched (G:A) versus matched (G:C) base pair. *J. Am. Chem. Soc. 127*, 13245−13252.
(33) Radhakrishnan, R., and Schlick, T. (2006) Correct and incorrect nucleotide incorporation pathways in DNA polymerase beta. *Biochem. Biophys. Res. Commun. 350*, 521−529.
(34) Werneburg, B. G., Ahn, J., Zhong, X., Hondal, R. J., Kraynov, V. S., and Tsai, M. D. (1996) DNA polymerase beta: pre-steady-state kinetic analysis and roles of arginine-283 in catalysis and fidelity. *Biochemistry 35*, 7041−7050.
(35) Dunlap, C. A., and Tsai, M. D. (2002) Use of 2-aminopurine and tryptophan fluorescence as probes in kinetic analyses of DNA polymerase beta. *Biochemistry 41*, 11226−11235.
(36) Bakhtina, M., Roettger, M. P., and Tsai, M. D. (2009) Contribution of the reverse rate of the conformational step to polymerase beta fidelity. *Biochemistry 48*, 3197−3208.
(37) Johnson, K. A., Simpson, Z. B., and Blom, T. (2009) Global kinetic explorer: a new computer program for dynamic simulation and fitting of kinetic data. *Anal. Biochem. 387*, 20−29.
(38) Johnson, K. A., Simpson, Z. B., and Blom, T. (2009) FitSpace explorer: an algorithm to evaluate multidimensional parameter space in fitting kinetic data. *Anal. Biochem. 387*, 30−41.
(39) Frey, C., Banyasz, J., and Stuehr, J. (1972) Interactions of divalent metal ions with inorganic and nucleoside phosphates. II. Kinetics of magnesium(II) with $HP_3O_{10}^{4-}$, ATP, CTP, $HP_2O_7^{3-}$, ADP, and CDP. *J. Am. Chem. Soc. 94*, 9198−9204.
(40) Pelletier, H., Sawaya, M. R., Kumar, A., Wilson, S. H., and Kraut, J. (1994) Structures of ternary complexes of rat DNA polymerase beta, a DNA template-primer, and ddCTP. *Science 264*, 1891−1903.
(41) Warshel, A. (1998) Electrostatic origin of the catalytic power of enzymes and the role of preorganized active sites. *J. Biol. Chem. 273*, 27035−27038.
(42) Bombarda, E., and Ullmann, G. M. (2010) pH-dependent pKa values in proteins--a theoretical analysis of protonation energies with practical consequences for enzymatic reactions. *J. Phys. Chem. B 114*, 1994−2003.
(43) Dixon, H. B., and Tipton, K. F. (1973) Negatively co-operative ligand binding. *Biochem. J. 133*, 837−842.
(44) Cleland, W. W. (1982) The use of pH studies to determine chemical mechanisms of enzyme-catalyzed reactions. *Methods Enzymol. 87*, 390−405.
(45) Johnson, K. A. (1992) Transient-state kinetic analysis of enzyme reaction pathways, in *The Enzymes* (Sigman, D. S., Ed.) 3rd ed., pp 2−62, Academic Press, Inc., San Diego, CA.
(46) Arora, K., and Schlick, T. (2005) Conformational transition pathway of polymerase beta/DNA upon binding correct incoming substrate. *J. Phys. Chem. B 109*, 5358−5367.
(47) Joyce, C. M., and Benkovic, S. J. (2004) DNA polymerase fidelity: kinetics, structure, and checkpoints. *Biochemistry 43*, 14317−14324.
(48) Radhakrishnan, R., and Schlick, T. (2004) Orchestration of cooperative events in DNA synthesis and repair mechanism unraveled by transition path sampling of DNA polymerase beta's closing. *Proc. Natl. Acad. Sci. U. S. A. 101*, 5970−5975.
(49) Batra, V. K., Beard, W. A., Shock, D. D., Pedersen, L. C., and Wilson, S. H. (2008) Structures of DNA polymerase beta with active-site mismatches suggest a transient abasic site intermediate during misincorporation. *Mol. Cell 30*, 315−324.
(50) Arora, K., Beard, W. A., Wilson, S. H., and Schlick, T. (2005) Mismatch-induced conformational distortions in polymerase beta support an induced-fit mechanism for fidelity. *Biochemistry 44*, 13328−13341.
(51) Showalter, A. K., and Tsai, M. D. (2002) A reexamination of the nucleotide incorporation fidelity of DNA polymerases. *Biochemistry 41*, 10571−10576.
(52) Luo, G., Wang, M., Konigsberg, W. H., and Xie, X. S. (2007) Single-molecule and ensemble fluorescence assays for a functionally important conformational change in T7 DNA polymerase. *Proc. Natl. Acad. Sci. U. S. A. 104*, 12610−12615.
(53) Roettger, M. P., Bakhtina, M., and Tsai, M. D. (2008) Mismatched and matched dNTP incorporation by DNA polymerase beta proceed via analogous kinetic pathways. *Biochemistry 47*, 9718−9727.
(54) Tang, K. H., Niebuhr, M., Tung, C. S., Chan, H. C., Chou, C. C., and Tsai, M. D. (2008) Mismatched dNTP incorporation by DNA polymerase beta does not proceed via globally different conformational pathways. *Nucleic Acids Res. 36*, 2948−2957.

(55) Koumanov, A., Ruterjans, H., and Karshikoff, A. (2002) Continuum electrostatic analysis of irregular ionization and proton allocation in proteins. *Proteins 46*, 85−96.

(56) Wang, L., Broyde, S., and Zhang, Y. (2009) Polymerase-tailored variations in the water-mediated and substrate-assisted mechanism for nucleotidyl transfer: insights from a study of T7 DNA polymerase. *J. Mol. Biol. 389*, 787−796.

(57) Castro, C., Smidansky, E., Maksimchuk, K. R., Arnold, J. J., Korneeva, V. S., Gotte, M., Konigsberg, W., and Cameron, C. E. (2007) Two proton transfers in the transition state for nucleotidyl transfer catalyzed by RNA- and DNA-dependent RNA and DNA polymerases. *Proc. Natl. Acad. Sci. U. S. A. 104*, 4267−4272.

(58) Castro, C., Smidansky, E. D., Arnold, J. J., Maksimchuk, K. R., Moustafa, I., Uchida, A., Gotte, M., Konigsberg, W., and Cameron, C. E. (2009) Nucleic acid polymerases use a general acid for nucleotidyl transfer. *Nat. Struct. Mol. Biol. 16*, 212−218.